Chemical Science

ROYAL SOCIETY OF CHEMISTRY

EDGE ARTICLE

View Article Online
View Journal

Cite this: DOI: 10.1039/d6sc03446b

All publication charges for this article have been paid for by the Royal Society of Chemistry

Strategic physicochemical tuning: amphiphilic polymers as molecular regulators of amyloid aggregation and cytotoxicity

Jimin Kwak,[a] Seongmin Park,[a] Youngjin Kim,[b] Yunha Hwang,[c] Seung Jae Lee,[cd] Jeung Gon Kim *[b] and Mi Hee Lim *[a]

Amyloidogenesis is a central pathological process in neurodegenerative disorders, yet general chemical principles that enable its predictive control are still insufficiently understood. Synthetic polymers offer a versatile and chemically tunable platform for modulating amyloid assembly; however, quantitative relationships linking polymer physicochemical properties to amyloidogenic pathways and biological outcomes remain poorly established. Here we present a systematic and quantitative framework that connects polymer composition to amyloid reactivity. By precisely tuning hydrophobicity, hydrophilicity, and net charge, and integrating polymer synthesis with computational, biochemical, and cellular analyses, we uncover clear structure–activity relationships governing interactions with amyloidogenic peptides and proteins, such as amyloid-β and α-synuclein. We show that balanced amphiphilic architectures, particularly hydrophobic–zwitterionic compositions, suppress fibrillization, redirect aggregation pathways, and reduce cellular membrane association, thereby attenuating cytotoxicity. In contrast, cationic-rich polymers promote aggregation *via* electrostatically driven mechanisms, while hydrophobic-dominant polymers exhibit minimal regulatory effects. Importantly, these composition-dependent behaviors are conserved across distinct amyloid systems, establishing a generalizable physicochemical framework in which the interplay between amphiphilicity and charge dictates amyloid reactivity and cellular responses. Overall, this work provides design principles for polymer-based chemical modulators and a broadly applicable strategy for controlling protein aggregation in neurodegenerative disease contexts.

Received 24th April 2026
Accepted 4th June 2026

DOI: 10.1039/d6sc03446b

rsc.li/chemical-science

Introduction

Peptides and proteins are inherently dynamic, populating ensembles of interconverting conformations in biological systems. Under pathological conditions, however, certain proteins misfold and self-assemble into highly ordered, β-sheet-rich fibrillar structures known as amyloids, species implicated in nearly 50 human diseases (Fig. 1a).[1,2] Among these, Alzheimer's disease (AD) and Parkinson's disease (PD) represent the most prevalent neurodegenerative disorders and are closely associated with the aggregation of amyloid-β (Aβ) and α-synuclein (α-Syn), respectively (Fig. 1b).[3,4]

Amyloidogenesis proceeds through a complex, multi-step pathway in which monomeric peptides or proteins nucleate, oligomerize, and elongate into protofibrils and mature fibrils.[3,5,6] Importantly, soluble oligomers and structured aggregates can aberrantly interact with cellular membranes and organelles, disrupt intracellular signaling networks, and ultimately induce neurotoxicity.[5,7,8] Although the accumulation of these toxic assemblies is a hallmark of AD and PD, the molecular determinants governing their formation and pathogenicity remain incompletely defined. Addressing this challenge requires chemical strategies that not only interrogate amyloid assembly pathways but also enable their rational modulation.

Designing such chemical reagents demands careful consideration of the physicochemical features that direct interactions with aggregation-prone peptides and proteins. Key parameters include: (i) hydrophobicity, which enables engagement with hydrophobic regions that drive self-assembly;[9–13] (ii) hydrophilicity, which promotes interactions with polar amino acid residues and ensures aqueous compatibility;[10,14–16] (iii) net charge, which dictates electrostatic attraction or repulsion;[17–20] and (iv) multivalency, which allows cooperative binding across multiple sites.[21,22] The interplay among these properties ultimately

[a]Department of Chemistry, Korea Advanced Institute of Science and Technology (KAIST), Daejeon 34141, Republic of Korea. E-mail: miheelim@kaist.ac.kr
[b]Department of Chemistry, Hanyang University, Seoul 04763, Republic of Korea. E-mail: jeunggonkim@hanyang.ac.kr
[c]Department of Chemistry, Jeonbuk National University, Jeonju 54896, Republic of Korea
[d]Institute for Molecular Biology and Genetics, Jeonbuk National University, Jeonju 54896, Republic of Korea

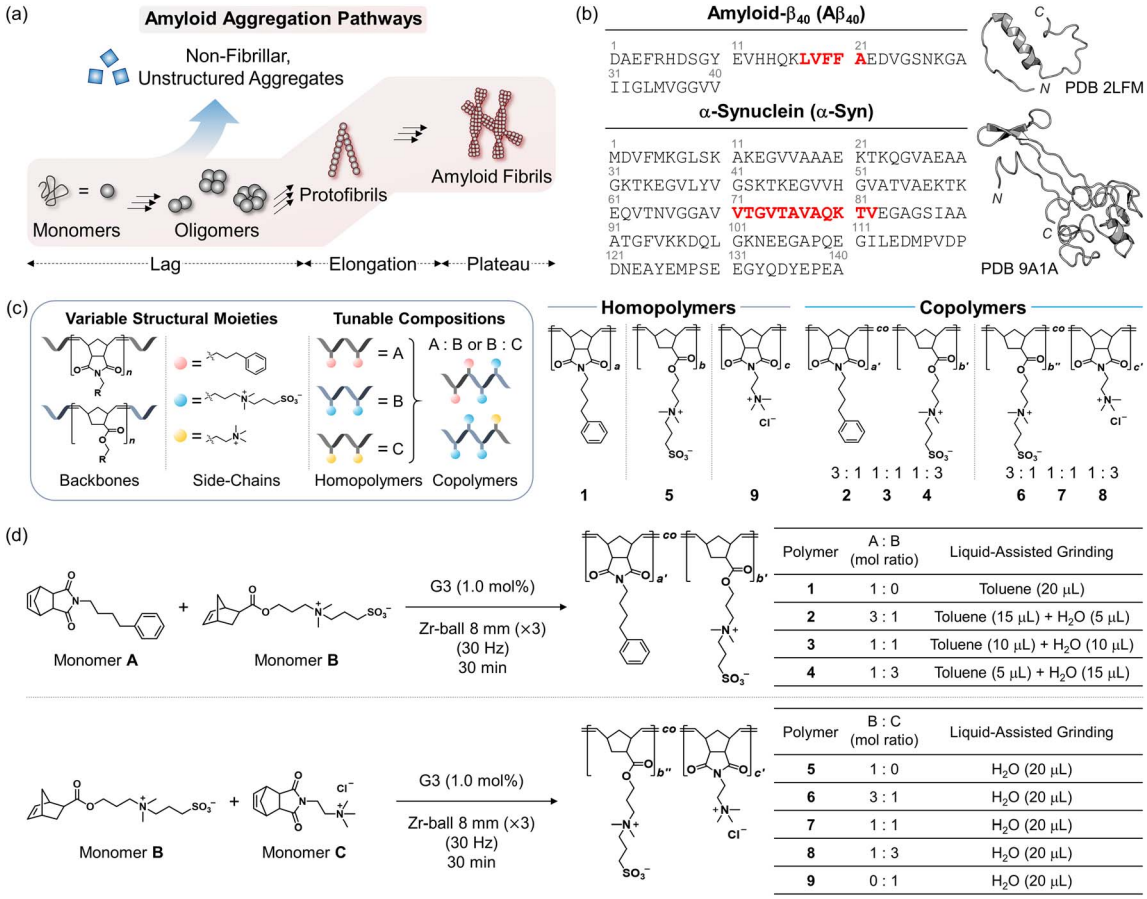

Polymer	A : B (mol ratio)	Liquid-Assisted Grinding
1	1 : 0	Toluene (20 μL)
2	3 : 1	Toluene (15 μL) + H_2O (5 μL)
3	1 : 1	Toluene (10 μL) + H_2O (10 μL)
4	1 : 3	Toluene (5 μL) + H_2O (15 μL)

Polymer	B : C (mol ratio)	Liquid-Assisted Grinding
5	1 : 0	H_2O (20 μL)
6	3 : 1	H_2O (20 μL)
7	1 : 1	H_2O (20 μL)
8	1 : 3	H_2O (20 μL)
9	0 : 1	H_2O (20 μL)

Fig. 1 Rational design and synthesis of polymers to control amyloidogenic aggregation and toxicity. (a) Schematic description of amyloid aggregation pathways. (b) Amino acid sequences and structures of $A\beta_{40}$ (PDB 2LFM[28]) or α-Syn (PDB 9A1A[29]). Amino acid residues critical for amyloidogenesis [*e.g.*, self-recognition site of $A\beta_{40}$ and non-Aβ component (NAC) core of α-Syn] are highlighted in bold and red. (c) Chemical structures of polymers **1**–**9** selected based on structural variations of backbones and side-chains. (d) Copolymerization of monomers.

determines whether a molecule suppresses, redirects, or accelerates amyloid aggregation.

Polymers provide a uniquely versatile platform for integrating these features within a single, tunable scaffold. Their modular architectures enable systematic control over molecular weight, backbone composition, side-chain functionality, amphiphilicity, and surface charge.[14,23,24] Amphiphilic polymers with hydrophobic backbones and hydrophilic side-chains have been shown to suppress amyloid fibril formation,[10] while incorporation of charged or functional moieties (*e.g.*, anionic, cationic, and zwitterionic groups, cholate, or fatty acids) further enhances amyloid–polymer interactions and modulates aggregation pathways.[12,18,19,25–27] Despite these advances, a key question remains: how does the quantitative balance between amphiphilicity and net charge within a polymer govern its reactivity towards amyloidogenic peptides or proteins? Clear structure–activity relationships (SARs) linking polymer composition to amyloid modulation remain elusive.

In this study, we address this challenge through the rational design and synthesis of a series of polymers with systesmatically varied backbone and side-chain compositions to finely tune amphiphilicity and net charge (Fig. 1c). By integrating computational modeling with biochemical and cellular investigations, we examined their interactions with Aβ and α-Syn and evaluated their effects on aggregation pathways and cytotoxicity. This approach enabled us to delineate direct relationships between polymer physicochemical parameters and their anti-amyloidogenic performance. Overall, our results demonstrate that the precise balance of amphiphilicity and net charge is a decisive determinant of polymer-mediated modulation of amyloid assembly and toxicity. These findings establish a rational chemical framework for the design of next-generation polymeric modulators targeting neurodegenerative proteinopathies.

Results and discussion

Rational selection and preparation of synthetic polymers

To systematically investigate how polymer physicochemical properties govern amyloid modulation, we designed a series of synthetic polymers in which hydrophobicity, hydrophilicity, and net charge were precisely controlled. Hydrophobic units were incorporated into the backbone to enable direct engagement with fibril-forming regions of amyloidogenic peptides and

proteins. Specifically, *N*-methyl-1,2-cyclopentane dicarboximide and methyl cyclopentanecarboxylate were selected as structural motifs to enhance interactions with hydrophobic peptide surfaces and promote cooperative multivalent contacts with aggregation-prone domains.[10,30] Onto these backbone frameworks, three chemically distinct side-chain functionalities were introduced to modulate intermolecular interactions: (i) propylbenzene, incorporated to promote π–π and C–H–π interactions with exposed aromatic and nonpolar residues, thereby shielding hydrophobic patches that drive amyloid self-association;[12,31] (ii) zwitterionic sulfobetaine groups, well-known antifouling motifs, exhibiting amino acid-like charge characteristics, introduced to modify interfacial and electrostatic properties through strong hydration shells, creating a steric-hydration barrier that stabilizes in solution and attenuates aggregation;[12,25,32,33] (iii) alkyl quaternary ammonium groups, providing permanent positive charges to enable electrostatic interactions with negatively charged Aβ and α-Syn (net charge of −3 and −9, respectively), thereby tuning local concentration effects and aggregation pathways.[18,20,34]

As summarized in Fig. 1c, by systematically varying the ratios of two backbone motifs and three side-chain moieties, we generated nine compositionally gradient polymers (**1–9**) spanning defined regimes of hydrophobicity, zwitterionic character, or cationic charge. This modular design enables fine control over amphiphilicity and net charge, allowing a quantitative assessment of how hydrophobic, hydration-mediated, and electrostatic contributions collectively dictate amyloid aggregation behavior. Polymers **1–9** were synthesized following previously reported procedures.[35,36] As outlined in Fig. 1d, mechanochemical ring-opening metathesis polymerization of norbornene monomers[35–37] was conducted under solid-state ball milling conditions using the Grubbs third generation catalyst. This approach enables efficient copolymerization of hydrophobic and hydrophilic monomers while minimizing limitations associated with the different solubility of monomers.[35,36] The solvent-minimized strategy afforded the polymers with controlled compositions. Detailed structural characterization is provided in Fig. S1–S5 and Table S1.

Potential binding modes of polymers with an amyloidogenic peptide or protein

Possible interactions between polymers **1–9** and $A\beta_{40}$ or α-Syn were investigated using molecular docking studies. Monomeric structures of $A\beta_{40}$ (PDB 2LFM[28]) and α-Syn (PDB 9A1A[29]), obtained from solution nuclear magnetic resonance (NMR) spectroscopy and time-resolved fluorescence resonance energy transfer-guided discrete molecular dynamics simulations, respectively, were employed as initial structural ensembles. Because evaluating the entire polymer chains is not feasible within typical docking workflows, shortened polymer fragments were used. Tetrameric units were selected as structural representations capable of preserving the experimentally defined monomer ratios and side-chain distributions of the copolymers (*e.g.*, 3 : 1 or 1 : 3 compositions) studied in this work. It should be noted that tetramers cannot fully reproduce the conformational and multivalent characteristics of full-length polymers and may therefore underestimate steric constraints and cooperative interactions inherent to larger polymer architectures. Nevertheless, previous computational studies on dendrimer–protein interactions have demonstrated that simplified molecular representations can still capture key interaction features despite differences in molecular size and multivalency.[38]

(i) Possible binding modes to $A\beta_{40}$. In the predicted $A\beta_{40}$–polymer heterodimers, as depicted in Fig. 2a and S6, polymers **8** and **9** were positioned within a pocket near the N-terminal and α-helical regions of $A\beta_{40}$ shown in Fig. 1b, whereas polymers **1–7** were located closer to the central portion of the peptide. To further characterize these binding patterns, the relative contact surface areas (CSAs) for $A\beta_{40}$ amino acid residues were calculated from the differences in solvent-accessible surface area values between polymer-free and polymer-bound $A\beta_{40}$, as summarized in Fig. 2b. The hydrophobic homopolymer **1** primarily interacted with amino acid residues located within the α-helical region of $A\beta_{40}$, including the hydrophobic self-recognition site, with minor extension towards the hydrophobic C-terminal region. Increasing the proportion of zwitterionic functionalities broadened the interaction interface, expanding CSAs across both the N-terminal and central regions of $A\beta_{40}$. In contrast, replacing zwitterionic units with cationic groups largely restricted the contact surface to the hydrophilic N-terminal region.

Residue-level interaction analysis revealed distinct binding modes depending on polymer composition. The hydrophobic polymer **1**, which contains fewer hydrogen-bond donor atoms than the other polymers, interacted with Aβ mainly through C–H–π interactions with His13 and Lys16, along with weak hydrogen bonding involving the side chains of His13 and Gln15 (Fig. 2a). Polymers enriched in zwitterionic functionalities, such as **3** and **5**, formed more extensive hydrogen-bonding networks. In polymer **3**, sulfonate groups participated in hydrogen bonding with the side chains of Asp1 (carboxylic acid), Lys16 (amino group), and Glu22 (carboxylic acid), as well as backbone amide and carbonyl groups spanning Ala2–Glu3, Asp23–Val24, Val24–Gly25, Gly25–Ser26, and Gly37–Gly38 (Fig. 2a). A comparable interaction pattern was observed for polymer **5**, whose sulfonate moieties formed hydrogen bonds with residues Arg5, Ser8, Lys16, Asp23, and Asn27, in addition to backbone amide groups between Ser8–Gly9 and Gly37–Gly38. Moreover, C–H–π interactions were detected: the benzene rings of polymer **3** engaged in hydrophobic interactions with Phe4, His13, and Gln15, whereas polymer **5** displayed a similar interaction between its backbone and imidazole ring of His13 (Fig. 2a).

Residues located near the β-turn motifs (Val12–Gln15 and Ala21–Asp23),[39,40] the self-recognition site (Leu17–Ala21),[41,42] the salt bridge (Lys16–Glu22),[43] and the C-terminal region (Ile32–Val40)[41,42] play crucial roles in structural transitions during Aβ fibrillization (Fig. 1b). Intermolecular contacts formed by polymers **3** and **5** within these regions may therefore perturb the conformation of Aβ and modulate its aggregation dynamics. In contrast, polymer **8** exhibited a more limited interaction profile, consisting primarily of hydrogen bonds involving Arg5 and

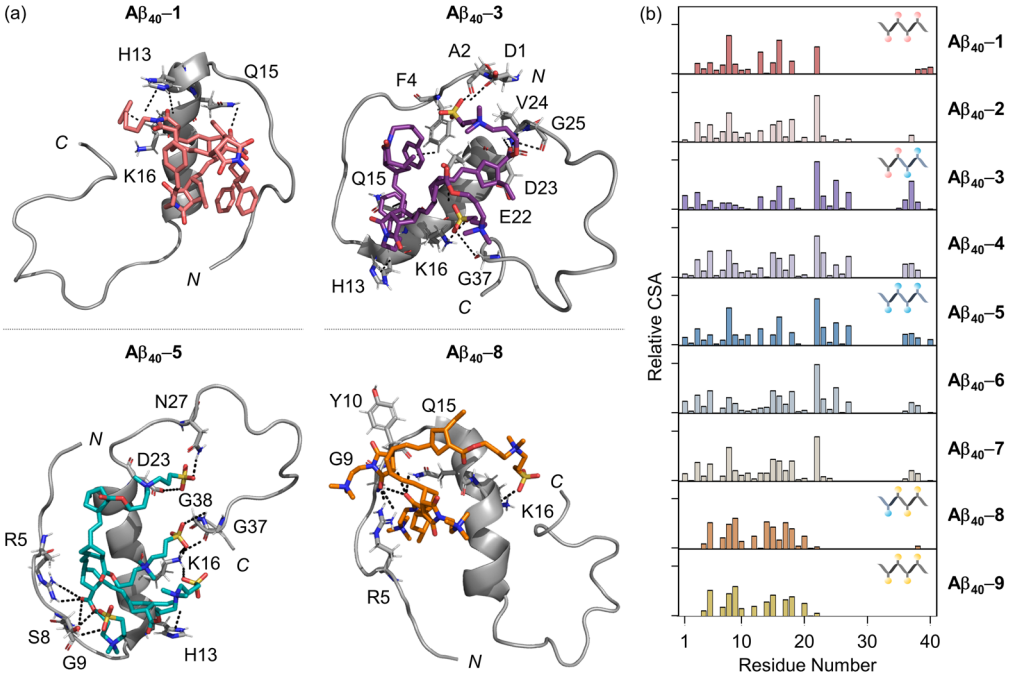

Fig. 2 Interactions of polymers **1–9** with $A\beta_{40}$ (PDB 2LFM[28]) analyzed by molecular docking simulations. (a) Putative binding modes of $A\beta_{40}$ with polymers **1**, **3**, **5**, and **8**. Hydrogen bonds (2.0–3.9 Å) and π–π or C–H–π interactions (2.7–3.7 Å) between polymers and $A\beta_{40}$ are indicated with dashed lines. H, N, O, and S atoms are indicated in white, blue, red, and yellow, respectively. (b) Relative CSAs of $A\beta_{40}$ amino acid residues upon binding to polymers **1–9**. Heterodimeric models used for calculating CSA values are enumerated in Fig. S6.

Gln15 as well as the backbone carbonyl and amide groups within the Gly9–Lys16 region (Fig. 2a).

(ii) Possible binding modes to α-Syn. We next examined potential interactions between the polymers and α-Syn, another aggregation-prone protein, as illustrated in Fig. 3a and S6. Docking simulations predicted that polymers **1** and **2** were positioned within the gap between the N- and C-terminal segments (Fig. 1b), whereas polymers **3–9** were located closer to the central domain and C-terminus of the protein. These binding patterns were consistent with relative CSA analyses calculated for each protein–polymer complex, as outlined in Fig. 3b. Hydrophobic-dominant polymers **1** and **2** displayed CSA distributions spanning both the N- and C-terminal regions. Increasing the hydrophilic zwitterionic or cationic functionalities in the polymer side-chains shifted the interaction interface towards the central region of the protein, corresponding to the NAC domain (Fig. 1b), which is critical for α-Syn aggregation,[44,45] as well as toward the negatively charged C-terminus.[46] Notably, the zwitterionic polymer **5** exhibited the largest CSA among the nine polymers.

Residue-level analyses further revealed distinct interaction modes between the polymers and α-Syn. Polymer **1** formed limited hydrogen bonds between its backbone *N*-methyl-1,2-cyclopentane dicarboximide unit and the side chains of Asp2, Glu13, Gln79, and Thr81. Similar to the docking results with $A\beta_{40}$, zwitterionic-rich polymers **3** and **5** displayed more extensive hydrogen-bonding networks mediated by their sulfonate groups. In the case of polymer **3**, hydrogen bonds were predicted with residues Thr92, Lys96, Lys97, and Ser129, in addition to a backbone amide group between Glu126 and Met127. Polymer **5** also formed hydrogen bonds with the side chains of Glu13, Lys45, Asn65, Lys80, Glu83, Thr92, and Tyr125, along with backbone amide and carbonyl groups spanning Ala78–Glu79 and Gly84–Ala85. In contrast, polymer **8** showed a more localized interaction pattern, forming hydrogen bonds with backbone amide groups between Thr81–Val82, Ala89–Ala90, and Tyr136–Glu137, while an additional sulfonate moiety interacted with the side chains of Tyr125 and Tyr133.

Collectively, these docking results indicate that the balance of hydrophobic, hydrophilicity, and net charge within the polymers governs their interaction interfaces with amyloidogenic peptides or proteins. These features shape the residue-level binding patterns and contact surfaces across key aggregation-prone regions. Consequently, polymer composition may influence the molecular networks that regulate amyloid assembly.

Effects of polymers on $A\beta_{40}$ aggregation dynamics

To determine the impact of polymers **1–9** on $A\beta_{40}$ aggregation, the formation of $A\beta_{40}$ aggregates was monitored using the 8-anilino-1-naphthalenesulfonate (ANS) fluorescence assay, which detects both fibrillar and non-fibrillar aggregates.[47] As shown in Fig. 4a, $A\beta_{40}$ alone exhibited a characteristic sigmoidal kinetic profile with lag, elongation, and plateau phases (Fig. 1a), indicative of nucleation-dependent amyloid fibril formation. Sigmoidal fitting yielded a lag time (t_{lag}) of 4.56 (±0.07) h and a half-time ($t_{1/2}$) of 6.40 (±0.03) h (Fig. 4b and Table S2). Among the homopolymers, the hydrophobic polymer **1** (Fig. 1c) showed

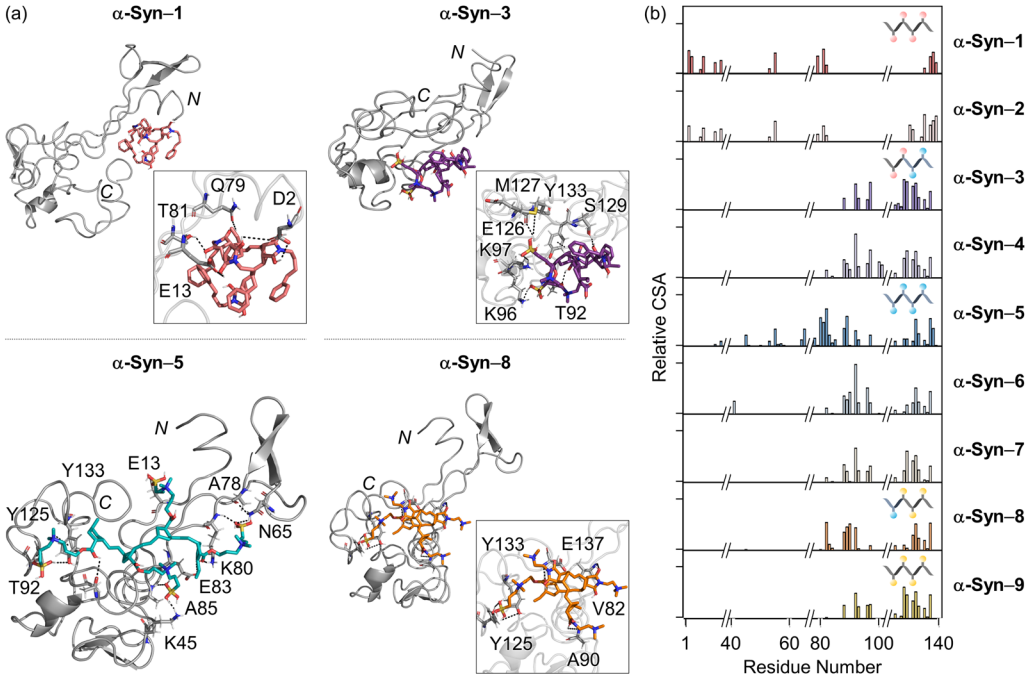

Fig. 3 Binding interfaces between polymers **1–9** and α-Syn (PDB 9A1A[29]) visualized by molecular docking simulations. (a) Possible α-Syn–polymer complexes for polymers **1**, **3**, **5**, and **8**. Hydrogen bonds (2.1–3.9 Å) and π–π or C–H–π interactions (2.7–3.7 Å) between polymers and α-Syn are indicated with dashed lines. H, N, O, and S atoms are indicated in white, blue, red, and yellow, respectively. (b) Relative CSAs of α-Syn amino acid residues upon binding to polymers **1–9**. Heterodimeric models used for calculating CSA values are enumerated in Fig. S6.

negligible effects in the t_{lag} and $t_{1/2}$ values even at its higher concentrations (Fig. 4b), indicating that hydrophobic interactions alone were insufficient to modulate aggregation kinetics. In contrast, the zwitterionic polymer **5** (Fig. 1c) noticeably delayed $A\beta_{40}$ aggregation in a dose-dependent manner ($A\beta_{40}$: polymer **5** = 1 : 1 – 1 : 10), increasing the t_{lag} values by 33.6 (±3.5) – 57.9 (±2.9)% and the $t_{1/2}$ values by 20.9 (±3.0) – 53.8 (±1.6)% relative to the control. This behavior reflects the resistance of zwitterionic moieties to peptide–peptide interactions, thereby suppressing $A\beta_{40}$ self-assembly.[32] By comparison, the cationic polymer **9** (Fig. 1c) shortened both kinetic parameters and enhanced ANS fluorescence intensity, suggesting accelerated aggregate formation.

Hydrophobic–zwitterionic copolymers (**2–4**; Fig. 1c) displayed a non-monotonic, inverted U-shaped trend of the t_{lag} and $t_{1/2}$ values as a function of concentration, with lag phase extensions ranging from 0.25 h to 3.64 h compared with $A\beta_{40}$ alone (Fig. 4b and c). This kinetic delay was accompanied by the reduced ANS fluorescence intensity, suggesting decreased aggregate accumulation. Within this subgroup, polymer **3** showed the strongest modulatory effect on $A\beta_{40}$ aggregation, reducing the intensity to 0.50 (±0.09) – 0.89 (±0.09)-fold and increasing the t_{lag} values by 67.6 (±3.3) – 79.8 (±4.0)% relative to the control, highlighting the importance of balanced hydrophobic–zwitterionic composition.

Conversely, zwitterionic–cationic copolymers (**6–8**; Fig. 1c) exhibited a progressive decrease in the t_{lag} and $t_{1/2}$ values with increasing cationic character, which became more pronounced at higher polymer concentrations (Fig. 4b and c). This kinetic profile was accompanied by an increase in ANS-reactive aggregates, ranging from 0.98 (±0.15) to 5.21 (±0.70)-fold. These results indicate that the incorporation of cationic functionalities promotes $A\beta_{40}$ aggregation, consistent with previous studies describing electrostatically driven acceleration of amyloid assembly.[18,34]

While the ANS fluorescence assay reports on overall aggregate formation, the extent of fibrillar assembly under these conditions remained unclear. To assess β-sheet-rich fibril formation, we performed the thioflavin-T (ThT) fluorescence assay, which selectively binds to cross-β structures.[48–50] As presented in Fig. 5a and Table S3, $A\beta_{40}$ alone displayed the expected sigmoidal profile, reaching a plateau after 8 h. Consistent with the results obtained by the ANS fluorescence assay, polymer **1** produced minimal kinetic changes but modestly increased the ThT fluorescence intensity by *ca.* 6–20%. Polymer **5**, however, significantly prolonged both kinetic parameters while reducing ThT fluorescence to 0.73 (±0.12) – 0.92 (±0.05)-fold, indicating the inhibition of β-sheet-rich aggregate formation. Polymer **9**, by comparison, facilitated $A\beta_{40}$ aggregation kinetics and increased the ThT fluorescence intensity, reflecting enhanced fibrillization.

The inverted U-shaped kinetic trends observed for copolymers **2–4** were also reproduced in the ThT fluorescence assay (Fig. 5b). Notably, polymer **3**, which contains a 1 : 1 ratio of hydrophobic and zwitterionic moieties, exhibited the strongest inhibitory effect, extending the t_{lag} and $t_{1/2}$ values by 1.39 (±0.10) – 3.38 (±0.08) h and 2.25 (±0.10) – 5.21 (±0.10) h, respectively, while reducing ThT-detectable aggregates. In

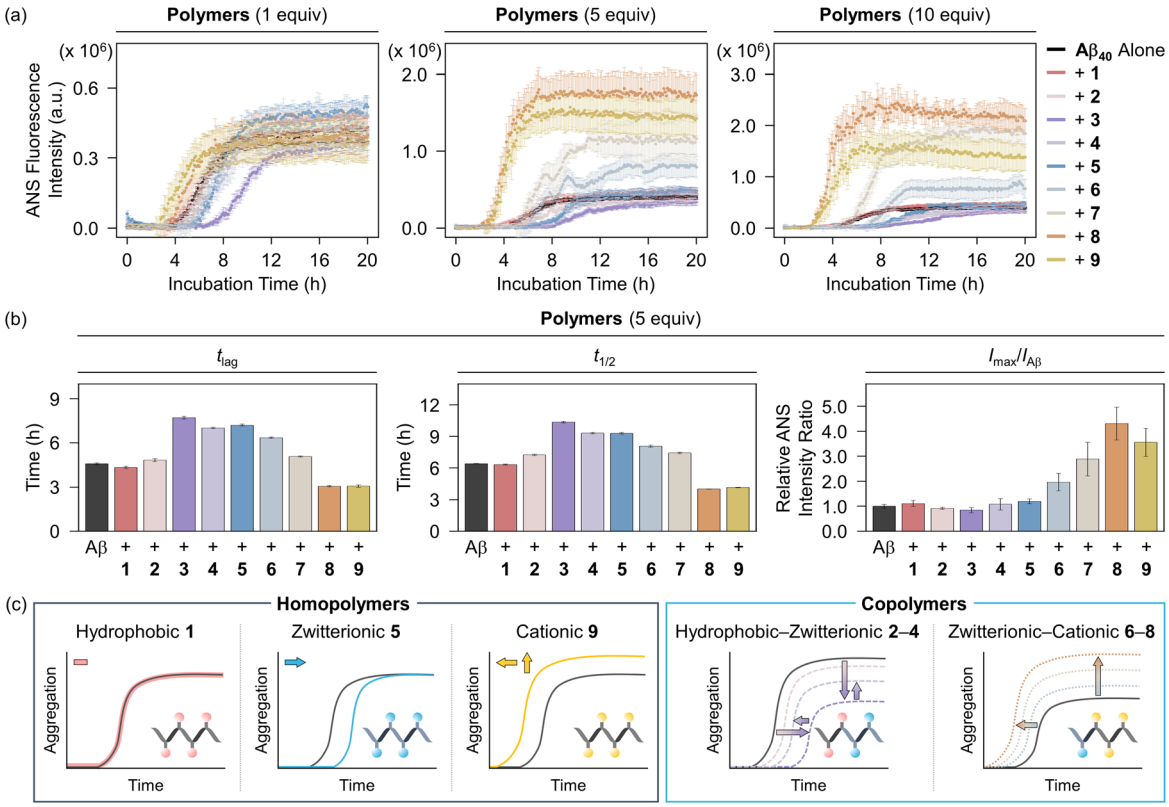

Fig. 4 Effects of polymers **1**–**9** on the formation of $A\beta_{40}$ aggregates. (a and b) Changes in $A\beta_{40}$ aggregation dynamics upon incubation with different concentrations of polymers analyzed by the ANS fluorescence assay. The fluorescence intensity was plotted as a function of incubation time and fitted to calculate kinetic parameters. Conditions: $[A\beta_{40}] = 10$ μM; [polymer] = 10, 50, or 100 μM (1% v/v DMSO); [ANS] = 10 μM; 20 mM HEPES, pH 7.4, 150 mM NaCl; 37 °C; quiescence; $\lambda_{ex} = 350$ nm; $\lambda_{em} = 480$ nm. Data are presented as mean ± s.e.m. (standard error of the mean) of three independent experiments. (c) Schematic summary of Aβ aggregation behavior upon incubation with polymers **1**–**9** monitored by the ANS fluorescence assay.

contrast, zwitterionic–cationic copolymers (**6**–**8**) induced monotonic acceleration of aggregation, with polymer **8** the showed the shortest lag phase [2.27 (±0.10) − 3.07 (±0.04) h] and the highest ThT fluorescence enhancement [1.15 (±0.08) − 3.36 (±0.35)-fold]. Interestingly, polymer **8** displayed stronger fibril-promoting effects than cationic polymer **9**, suggesting that aggregation behavior may be influenced not only by positive charge density but also by polymer packing characteristics reflected in hydrodynamic radius (Table S1), side-chain compositions (Fig. 1c), as well as the overall electrostatic balance of the Aβ–polymer complexes.

These effects were further corroborated by transmission electron microscopy (TEM). As depicted in Fig. 5c and S7, $A\beta_{40}$ alone formed branched fibrils, whereas polymer **1** preserved fibril morphology, polymer **5** produced thinner and fragmented fibrils, and polymer **9** yielded shortened and branched structures. In the presence of hydrophobic–zwitterionic copolymers **2**–**4**, heterogeneous assemblies composed of both fibrils and amorphous aggregates were observed, consistent with partial disruption of β-sheet formation monitored by the ThT fluorescence assay. For zwitterionic–cationic copolymers **6**–**8**, dense fibrillar bundles were generated, supporting their aggregation-promoting behavior detected in kinetic assays.

Collectively, our results demonstrate that the physicochemical balance of polymers governs their reactivity toward $A\beta_{40}$ and establishes distinct SARs across the polymer series. As summarized in Fig. 5d, the homopolymers define the individual roles of hydrophobic, zwitterionic, and cationic functionalities in modulating $A\beta_{40}$ aggregation. Hydrophobic interactions alone exerted minimal impact on aggregation kinetics, while zwitterionic functionalities delayed nucleation-dependent fibrillization, and cationic groups accelerated electrostatically-driven assembly. The behaviors of hydrophobic–zwitterionic (**2**–**4**) and zwitterionic–cationic (**6**–**8**) copolymers further reveal that precise tuning of overall amphiphilicity and net charge directs both the extent and direction of aggregation modulation. In particular, the overall electrostatic balance of the resulting Aβ–polymer complexes may additionally influence intermolecular interactions and aggregation kinetics. Notably, polymer **3** exhibited the strongest inhibitory effect, underscoring the importance of balanced hydrophobic–hydrophilic interactions in regulating amyloid fibril formation. In contrast, polymer **8** displayed the most pronounced aggregation-promoting behavior, highlighting the contribution of charge density to assembly. Taken together, these findings indicate that the effective modulation of Aβ self-assembly requires

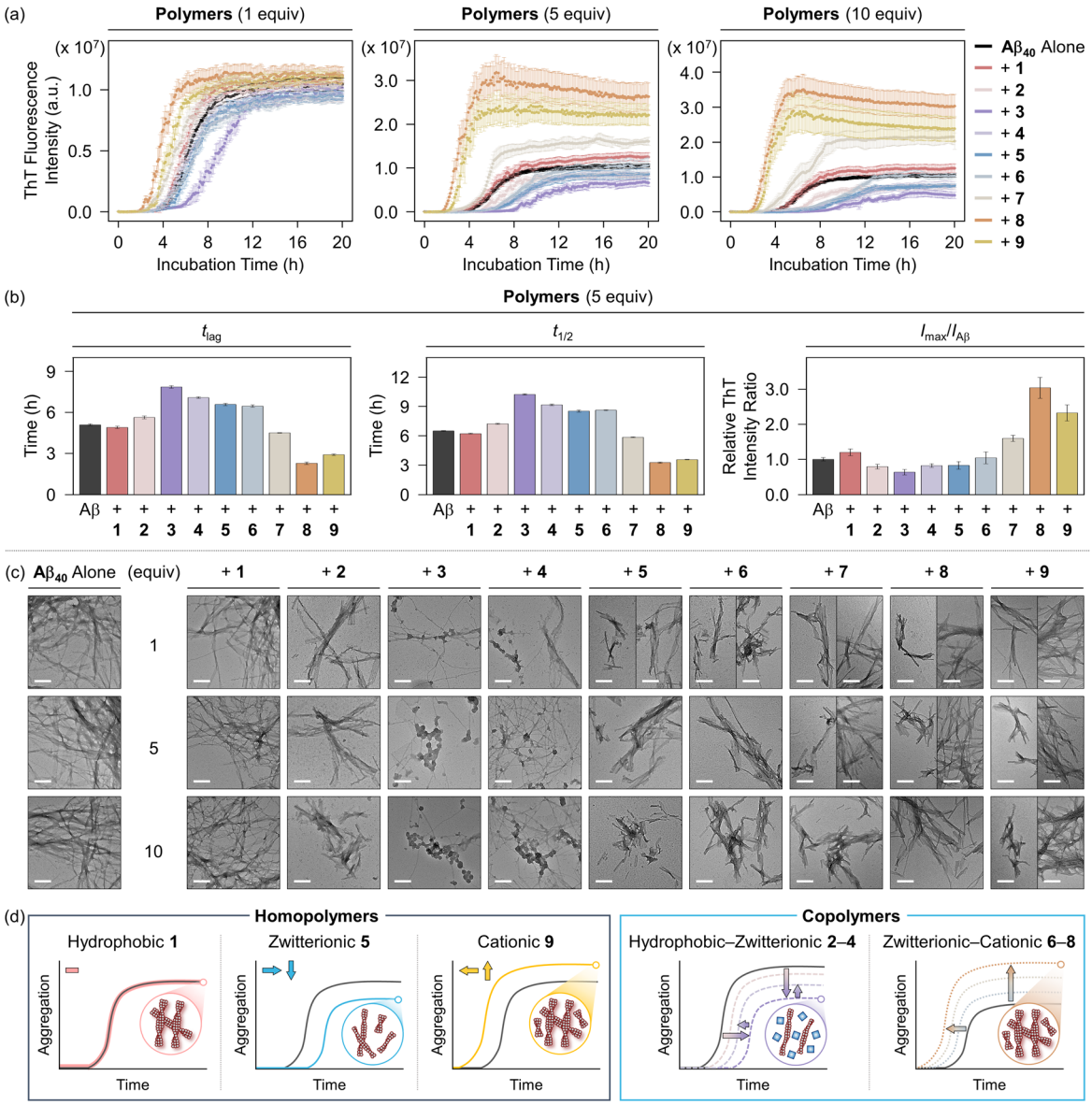

Fig. 5 Impact of polymers **1**–**9** on $A\beta_{40}$ fibrillation and morphology. (a and b) Formation of β-sheet-rich $A\beta_{40}$ aggregates upon exposure to polymers monitored by the ThT fluorescence assay. The fluorescence intensity was plotted as a function of incubation time and fitted to calculate kinetic parameters. Conditions: $[A\beta_{40}] = 10$ μM; [polymer] = 10, 50, or 100 μM (1% v/v DMSO); [ThT] = 10 μM; 20 mM HEPES, pH 7.4, 150 mM NaCl; 37 °C; quiescence; $\lambda_{ex} = 440$ nm; $\lambda_{em} = 490$ nm. Data are presented as mean ± s.e.m. of three independent experiments. (c) Morphology of the resultant $A\beta_{40}$ aggregates produced with and without polymers visualized by TEM. Conditions: $[A\beta_{40}] = 10$ μM; [polymer] = 10, 50, or 100 μM (1% v/v DMSO); 20 mM HEPES, pH 7.4, 150 mM NaCl; 24 h incubation; 37 °C; quiescence. Scale bar = 200 nm. (d) Schematic overview of the changes in $A\beta_{40}$ fibrillization by polymers **1**–**9**.

a finely balanced interplay among hydrophobicity, hydrophilicity, and net charge.

Reactivity of polymers toward α-Syn aggregation

To investigate whether the modulatory effects observed for Aβ extend to other amyloidogenic systems, we examined the effect of the polymers on the aggregation of α-Syn, an amyloidogenic protein associated with PD.[3,4] Aggregation dynamics were monitored using the ANS and ThT fluorescence assays, complemented by TEM analysis. Representative polymers (**1**, **3**, **5**, and **8**; structures shown in Fig. 1c) were selected based on their impact on $A\beta_{40}$ aggregation: hydrophobic polymer **1** (minimal effect on aggregation kinetics), zwitterionic polymer **5** (partial suppression of aggregation), hydrophobic–zwitterionic copolymer **3** (strongest inhibitory effect) and zwitterionic–cationic copolymer **8** (fastest aggregation kinetics).

As shown in Fig. 6a, α-Syn alone reached a plateau after 24 h, as analyzed by the ANS fluorescence assay, which detects both fibrillar and non-fibrillar aggregates.[47] Treatment with polymer **1** resulted in no significant changes in kinetic parameters, consistent with its behavior in $A\beta_{40}$ aggregation. Similarly, polymer **5** induced only minor decreases in the t_{lag} and $t_{1/2}$

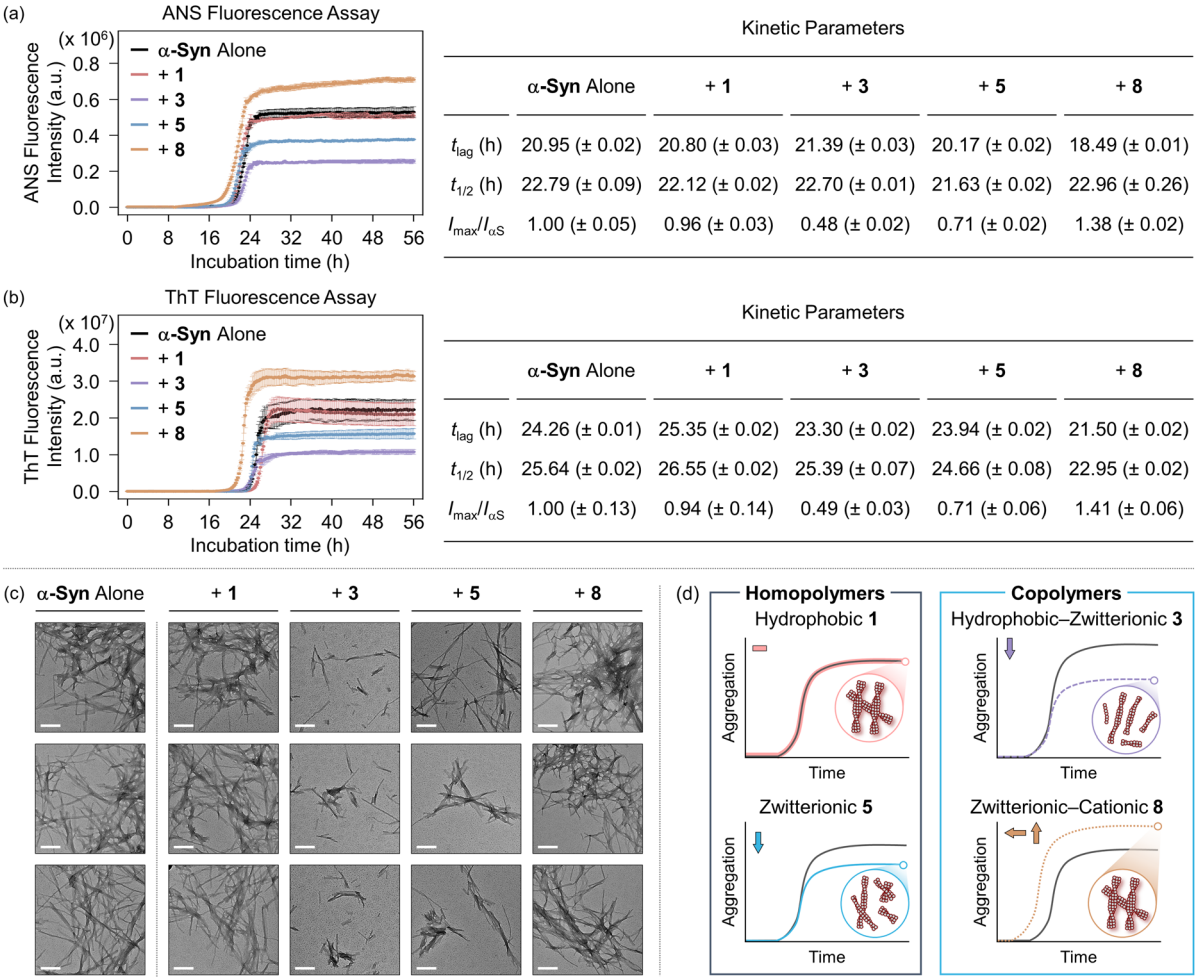

Kinetic Parameters

	α-Syn Alone	+ 1	+ 3	+ 5	+ 8
t_{lag} (h)	20.95 (± 0.02)	20.80 (± 0.03)	21.39 (± 0.03)	20.17 (± 0.02)	18.49 (± 0.01)
$t_{1/2}$ (h)	22.79 (± 0.09)	22.12 (± 0.02)	22.70 (± 0.01)	21.63 (± 0.02)	22.96 (± 0.26)
$I_{max}/I_{\alpha S}$	1.00 (± 0.05)	0.96 (± 0.03)	0.48 (± 0.02)	0.71 (± 0.02)	1.38 (± 0.02)

Kinetic Parameters

	α-Syn Alone	+ 1	+ 3	+ 5	+ 8
t_{lag} (h)	24.26 (± 0.01)	25.35 (± 0.02)	23.30 (± 0.02)	23.94 (± 0.02)	21.50 (± 0.02)
$t_{1/2}$ (h)	25.64 (± 0.02)	26.55 (± 0.02)	25.39 (± 0.07)	24.66 (± 0.08)	22.95 (± 0.02)
$I_{max}/I_{\alpha S}$	1.00 (± 0.13)	0.94 (± 0.14)	0.49 (± 0.03)	0.71 (± 0.06)	1.41 (± 0.06)

Fig. 6 Impact of polymers on the aggregation of α-Syn. (a) Aggregation kinetics of α-Syn upon incubation with and without polymers monitored by the ANS fluorescence assay. (b) Formation of β-sheet-rich aggregates in the sample of α-Syn incubated with and without polymers traced by the ThT fluorescence assay. The fluorescence intensity was plotted as a function of incubation time and fitted to calculate kinetic parameters. Conditions: [α-Syn] = 100 μM; [polymer] = 200 μM (1% v/v DMSO); [ANS] = 10 μM; [ThT] = 10 μM; 400 mM NaPi, pH 7.4, 150 mM NaCl; 37 °C; 3 mm beads; quiescence; (for the ANS fluorescence assay) λ_{ex} = 350 nm; λ_{em} = 480 nm; (for the ThT fluorescence assay) λ_{ex} = 440 nm; λ_{em} = 490 nm. Data are presented as mean ± s.e.m. of three independent experiments. (c) Morphology of the resultant protein aggregates monitored by TEM. Conditions: [α-Syn] = 100 μM; [polymer] = 200 μM (1% v/v DMSO); 400 mM NaPi, pH 7.4, 150 mM NaCl; 56 h incubation; 37 °C; 3 mm beads; quiescence. Scale bar = 200 nm. (d) Schematic overview of α-Syn aggregation studies.

values [3.7 (±0.1)% and 5.1 (±0.4)%, respectively], while reducing ANS-reactive aggregates by 29.0 (±5.4)%, suggesting partial inhibition *via* protein–zwitterionic interactions.[32]

In contrast, copolymer **3** induced a modest delay in the t_{lag} value of 0.44 h, along with a 0.48 (±0.03)-fold decrease in the ANS fluorescence intensity. These results indicate the effective modulation of α-Syn aggregation through balanced hydrophobic and zwitterionic characters. Conversely, copolymer **8** accelerated aggregation, reducing the t_{lag} value by 11.7 (±0.1)% and increasing aggregate formation by 38.0 (±5.4)%, highlighting the role of cationic functionalities in promoting α-Syn assembly.

To further quantify the formation of β-sheet-rich aggregates, the ThT fluorescence assay was performed. Consistent with the results obtained by the ANS fluorescence assay, as presented in Fig. 6b, polymer **5** and copolymer **3** did not significantly alter kinetic parameters but reduced fibril formation by 29.0 (±14.3)% and 51.0 (±13.3)%, respectively. Different from polymers **3** and **5**, copolymer **8** accelerated aggregation, decreasing the t_{lag} and $t_{1/2}$ values of 2.76 (±0.02) h and 2.69 (±0.03) h, respectively, and increasing the ThT fluorescence intensity by 1.41 (±0.19)-fold, confirming its aggregation-promoting effect.

Polymer **1** produced only minimal changes in fibrillization, with slight increases in the t_{lag} and $t_{1/2}$ values [4.5 (±0.1)% and 3.6 (±0.1)%, respectively]. TEM analysis further supported these findings (Fig. 6c). α-Syn alone formed dense, highly branched fibrils, which were similarly observed in the presence of polymers **1** and **8**. In contrast, polymer **5** produced thinner, shorter filamentous structures, whereas polymer **3** yielded markedly shorter and more fragmented fibrils, consistent with reduced fibril formation.

Collectively, these results demonstrate that the balance of hydrophobicity, hydrophilicity, and charge governs polymer-mediated modulation of α-Syn aggregation, with both similarities and differences compared to $A\beta_{40}$. As outlined in Fig. 6d,

hydrophobic polymer **1** exerted minimal influence, whereas zwitterionic polymer **5** and hydrophobic–zwitterionic copolymer **3** reduced aggregate formation with limited effects on kinetics, indicating that zwitterionic functionalities primarily affect the aggregate yield rather than nucleation. Notably, the significant inhibitory impact of polymer **3** highlights the importance of balancing hydrophobic and zwitterionic moieties. Cationic copolymer **8** accelerated aggregation and enhanced fibril formation, in line with electrostatically-driven aggregation.

Interestingly, the extent of kinetic modulation was less pronounced for α-Syn than for $A\beta_{40}$. This difference likely arises from intrinsic properties of α-Syn, including its sequence length, charge distribution, and intrinsically disordered nature, which may limit the extent to which external interactions perturb nucleation kinetics.[10] Overall, these findings establish amphiphilicity and net charge as general design parameters for modulating amyloid assembly, while highlighting protein-specific responses that enable selective control over distinct aggregation pathways.

Impact of polymers on the toxicity associated with $A\beta_{40}$ and α-Syn in living cells

To evaluate the cytotoxicity of the resultant $A\beta_{40}$ and α-Syn aggregates formed in the presence of polymers, the MTT assay [MTT = 3-(4,5-dimethylthiazol-2-yl)-2,5-diphenyltetrazolium bromide] was performed employing human neuroblastoma SH-SY5Y (5Y) cells. As shown in Fig. 7a, cells were treated with amyloid species alone or with the samples pre-incubated with representative polymers **1**, **3**, **5**, and **8** (structures shown in Fig. 1c), selected based on their distinct aggregation-modulating behaviors. Prior to evaluating $A\beta_{40}$-mediated toxicity, the intrinsic cytotoxicity of the polymers was assessed (Fig. S8). Polymers **1–5** exhibited minimal toxicity under the concentrations used for $A\beta_{40}$ studies (>80% cell viability), whereas cationic polymers **6–9** reduced cell viability by *ca.* 17–29%, likely due to the membrane disruption arising from electrostatic interactions between cationic structural moieties and negatively charged cell surfaces.

When $A\beta_{40}$ species pre-incubated with polymers were applied to cells, distinct cytotoxic responses were observed (Fig. 7a). Consistent with its negligible effect on aggregation, polymer **1** did not significantly alter cell viability relative to $A\beta_{40}$ alone. In the case of polymers **3** and **5**, cell viability was increased by 7.0 (±1.0) − 11.6 (±1.2)%, indicating attenuation of $A\beta_{40}$-induced toxicity. Moreover, polymer **8** further reduced viability by 7.5 (±0.9) − 8.6 (±1.0)%, suggesting exacerbation of toxicity mediated by $A\beta_{40}$.

A similar analysis was carried out for α-Syn (Fig. 7b). Polymer-only controls showed negligible toxicity (>93%

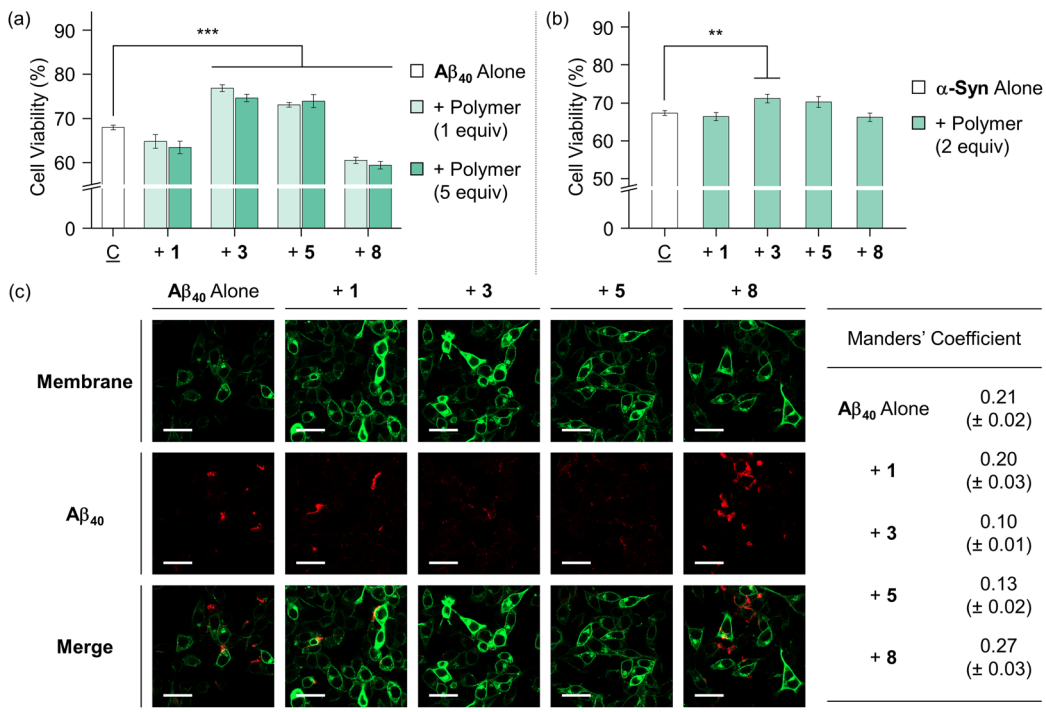

Fig. 7 Effects of polymers **1–9** on the toxicity induced by $A\beta_{40}$ and α-Syn in living cells. Cell viability (%) upon treatment of (a) $A\beta_{40}$ or (b) α-Syn incubated with and without polymers are determined by the MTT assay, respectively. Viability was calculated relative to that of cells treated with an equivalent amount of the buffered solution with 1% v/v DMSO. Lane C: $A\beta_{40}$ or α-Syn alone. Conditions: (for $A\beta_{40}$ experiments) $[A\beta_{40}] = 10$ μM; [polymer] = 10 or 50 μM (1% v/v DMSO); 20 mM HEPES, pH 7.4, 150 mM NaCl; 37 °C; quiescence; post-incubation for 24 h; (for α-Syn experiments) [α-Syn] = 10 μM; [polymer] = 20 μM (1% v/v DMSO); 400 mM NaPi, pH 7.4, 150 mM NaCl; 37 °C; 3 mm beads; quiescence; pre- and post-incubation for 56 h and 24 h, respectively. $^{**}P < 0.01$; $^{***}P < 0.001$; Student's *t*-test. Data are presented as mean ± s.e.m. of three independent experiments. (c) Cellular membrane interactions upon treatment of $A\beta_{40}$ incubated with and without polymers analyzed by ICC measurements. Conditions: $[A\beta_{40}] = 10$ μM; [polymer] = 50 μM (1% v/v DMSO); 20 mM HEPES, pH 7.4, 150 mM NaCl; 37 °C; quiescence; pre- and post-incubation for 24 h. Scale bar = 30 μm.

viability; Fig. S8). Polymer **1** did not mitigate α-Syn-induced cytotoxicity, consistent with its minimal effect on aggregation. Polymers **3** and **5** produced modest improvements in cell viability [5.7 (±1.9)% and 4.4 (±1.0)%, respectively], although these effects were less pronounced than for $A\beta_{40}$. In contrast, polymer **8** did not significantly affect α-Syn-mediated cytotoxicity.

Because amyloid aggregates can induce toxicity through membrane association and disruption of cellular signaling,[5,51] we next examined whether the observed cytotoxicity trends correlate with membrane interactions. As described in Fig. 7c, immunocytochemistry (ICC) studies were performed in 5Y cells,[52] focusing on $A\beta_{40}$ due to its more notable polymer-dependent effects. Cell membranes were stained with a fluorescent membrane dye, $A\beta_{40}$ species were detected using a fluorophore-conjugated anti-Aβ antibody (6E10). Co-localization between $A\beta_{40}$ and cell membranes was quantified using the Manders' coefficient,[53] which represents the fraction of $A\beta_{40}$ fluorescence overlapping with membrane staining.

In the absence of polymers, the Manders' coefficient was measured to be 0.21 (±0.02), as shown in Fig. 7c. Consistent with its minimal impact on $A\beta_{40}$ aggregation and cytotoxicity, polymer **1** did not significantly alter $A\beta_{40}$–cellular membrane association. In contrast, aggregation-regulating polymers **3** and **5** reduced $A\beta_{40}$–membrane interactions by 52.4 (±10.0)% and 38.1 (±13.0)%, respectively, indicating the formation of assemblies with a lower membrane affinity. This decrease correlates with the observed improvements in cell viability (Fig. 7a). As for polymer **8**, an aggregation-accelerator, increased the Manders' coefficient, suggesting enhanced membrane interactions likely due to increased aggregate formation.

Together, these results demonstrate that polymer composition governs both the cytotoxicity and membrane activity of amyloid assemblies. Polymers that suppress fibrillization reduce membrane association and improve cell viability, whereas aggregation-promoting polymers enhance membrane interactions and exacerbate toxicity. For α-Syn, the comparatively modest modulating of aggregation kinetics is reflected in weaker cellular responses; nevertheless, polymers that reduce aggregate formation modestly alleviate cytotoxicity. Overall, these findings establish a direct correlation between polymer-modulated aggregation pathways and amyloid-induced cellular outcomes.

Conclusions

Amyloid assembly is a dynamic and heterogeneous process governed by complex, multistep pathways, making its predictive control a longstanding challenge. In this study, we establish a chemically programmable polymer platform in which systematic tuning of hydrophobic, zwitterionic, and cationic features enables precise regulation of amyloid aggregation and cytotoxicity across both $A\beta_{40}$ and α-Syn systems. Integrated computational and experimental investigations reveal that polymer composition dictates distinct interaction modes and downstream biological outcomes. Hydrophobic components engage aggregation-prone regions but are insufficient on their own to alter assembly pathways; zwitterionic functionalities introduce hydration- and hydrogen-bonding networks that suppress fibrillization and cellular membrane interactions; and cationic moieties promote electrostatically-driven aggregation and exacerbate toxicity. Notably, copolymers uncover a non-linear, composition-dependent regime in which balanced amphiphilic architectures achieve optimal inhibition of amyloid assembly and cytotoxicity.

These findings establish a clear physicochemical framework in which the interplay between amphiphilicity and net charge governs amyloid–polymer reactivity and cellular responses. Beyond defining SARs, this work advances a key design principle: precise compositional balance, not maximal functionality, determines effective control over pathological protein assembly. More broadly, this study positions synthetic polymers as modular chemical systems for reprogramming protein aggregation landscapes. The principles established here provide a generalizable foundation for engineering next-generation materials and chemical reagents to interrogate and therapeutically target protein misfolding disorders.

Author contributions

J. K., J. G. K., and M. H. L. designed the research. J. K. performed docking simulations, TEM, and cell studies using the MTT assay with data analysis. J. K. and S. P. carried out biochemical assays and ICC studies. Y. K. and J. G. K. synthesized all polymers tested in this work. S. P., Y. H., and S. J. L. conducted the expression and purification of α-Syn. J. K., S. P., and M. H. L. wrote the manuscript with input from all authors.

Conflicts of interest

There are no conflicts to declare.

Data availability

All experimental details and data supporting the findings of this study are available within the paper and its supplementary information (SI). The data are also available from the corresponding authors upon reasonable request. Supplementary information: experimental section, Tables S1–S3, and Fig. S1–S8. See DOI: https://doi.org/10.1039/d6sc03446b.

Acknowledgements

This work was supported by the National Research Foundation of Korea (NRF) grant funded by the Korean government {Creative Research Initiative [RS-2022-NR070709 (M. H. L.)]; Global Science Research Center Program [RS-2024-00411134 (M. H. L.)]; RS-2024-00342198 (J. G. K.)} and the Yangyoung Foundation (J. G. K.). This work was also supported by the Regional Innovation System & Education (RISE) program [2025-RISE-13-JBU (S. J. L.)] through the Jeonbuk RISE Center funded by the

Ministry of Education and the Jeonbuk State. J. K. thanks the NRF PhD fellowship grant (RS-2024-00407337).

Notes and references

1 T. P. J. Knowles, M. Vendruscolo and C. M. Dobson, *Nat. Rev. Mol. Cell Biol.*, 2014, **15**, 384.
2 F. Chiti and C. M. Dobson, *Annu. Rev. Biochem.*, 2006, **75**, 333.
3 M. G. Savelieff, G. Nam, J. Kang, H. J. Lee, M. Lee and M. H. Lim, *Chem. Rev.*, 2019, **119**, 1221.
4 D. Li and C. Liu, *Nat. Rev. Neurosci.*, 2022, **23**, 523.
5 S. J. C. Lee, E. Nam, H. J. Lee, M. G. Savelieff and M. H. Lim, *Chem. Soc. Rev.*, 2017, **46**, 310.
6 C. Na, Y. Jang, M. Son and M. H. Lim, *ACS Appl. Mater. Interfaces*, 2026, **18**, 9285.
7 D. J. Rinauro, F. Chiti, M. Vendruscolo and R. Limbocker, *Mol. Neurodegener.*, 2024, **19**, 20.
8 J. Kwak, J. Woo, S. Park and M. H. Lim, *J. Inorg. Biochem.*, 2023, **238**, 112053.
9 F. Chiti, M. Stefani, N. Taddei, G. Ramponi and C. M. Dobson, *Nature*, 2003, **424**, 805.
10 S.-Y. Ow, I. Bekard, A. Blencowe, G. G. Qiao and D. E. Dunstan, *J. Mater. Chem. B*, 2015, **3**, 1350.
11 D. D. Sahtoe, E. A. Andrzejewska, H. L. Han, E. Rennella, M. M. Schneider, G. Meisl, M. Ahlrichs, J. Decarreau, H. Nguyen, A. Kang, P. Levine, M. Lamb, X. Li, A. K. Bera, L. E. Kay, T. P. J. Knowles and D. Baker, *Nat. Chem. Biol.*, 2024, **20**, 981.
12 R. Rajan, Y. Suzuki and K. Matsumura, *Macromol. Biosci.*, 2018, **18**, 1800016.
13 C. Na, J. Lee, J.-M. Suh, J. Go, J. Kwak, J. Lee, K.-S. Kim, C.-H. Lee, M. Kim and M. H. Lim, *J. Am. Chem. Soc.*, 2026, **148**, 461.
14 Rupali, B. Joseph, S. Thomas, N. Sen, A. Paschold, W. H. Binder and S. Kumar, *Polym. Chem.*, 2023, **14**, 392.
15 J. Kwak, Y. Yi, S. Park and M. H. Lim, *Chem. Sci.*, 2025, **16**, 889.
16 S. Park, M. Kim, Y. Lin, M. Hong, G. Nam, A. Mieczkowski, J. Kardos, Y.-H. Lee and M. H. Lim, *Chem. Sci.*, 2023, **14**, 9293.
17 S. Palmal, N. R. Jana and N. R. Jana, *J. Phys. Chem. C*, 2014, **118**, 21630.
18 A. Assarsson, S. Linse and C. Cabaleiro-Lago, *Langmuir*, 2014, **30**, 8812.
19 K. M. Montgomery, E. C. Carroll, A. C. Thwin, A. Y. Quddus, P. Hodges, D. R. Southworth and J. E. Gestwicki, *J. Am. Chem. Soc.*, 2023, **145**, 3926.
20 J. Goers, V. N. Uversky and A. L. Fink, *Protein Sci.*, 2003, **12**, 702.
21 P. M. H. Heegaard, U. Boas and D. E. Otzen, *Macromol. Biosci.*, 2007, **7**, 1047.
22 B. Klajnert, M. Cortijo-Arellano, J. Cladera and M. Bryszewska, *Biochem. Biophys. Res. Commun.*, 2006, **345**, 21.
23 M. Holubová, P. Štěpánek and M. Hrubý, *Colloid Polym. Sci.*, 2021, **299**, 343.
24 P. Ghosh and P. De, *ACS Appl. Bio Mater.*, 2020, **3**, 6598.
25 R. Rajan and K. Matsumura, *J. Mater. Chem. B*, 2015, **3**, 5683.
26 D. Ghosh, S. Bag and P. De, *Bioconjug. Chem.*, 2025, **36**, 1040.
27 A. Bera, D. Mukhopadhyay, K. Goswami, P. Ghosh, R. De and P. De, *Biomater. Sci.*, 2022, **10**, 3466.
28 S. Vivekanandan, J. R. Brender, S. Y. Lee and A. Ramamoorthy, *Biochem. Biophys. Res. Commun.*, 2011, **411**, 312.
29 J. Chen, S. Zaer, P. Drori, J. Zamel, K. Joron, N. Kalisman, E. Lerner and N. V. Dokholyan, *Structure*, 2021, **29**, 1048.
30 K. P. Carrow, H. L. Hamilton, M. P. Hopps, Y. Li, B. Qiao, N. C. Payne, M. P. Thompson, X. Zhang, A. Magassa, M. Fattah, S. Agarwal, M. P. Vincent, M. Buyanova, P. A. Bertin, R. Mazitschek, M. Olvera de la Cruz, D. A. Johnson, J. A. Johnson and N. C. Gianneschi, *Adv. Mater.*, 2024, **36**, 2311467.
31 X. Dai, D. Zhao, K. Matsumura and R. Rajan, *ACS Appl. Bio Mater.*, 2023, **6**, 2738.
32 R. Rajan, T. Furuta, D. Zhao and K. Matsumura, *Cell Rep. Phys. Sci.*, 2024, **5**, 102012.
33 Z. Zeng, S. Chen and Y. Chen, *ChemMedChem*, 2023, **18**, e202300245.
34 R. Sternke-Hoffmann, X. Sun, A. Menzel, M. D. S. Pinto, U. Venclovaite, M. Wördehoff, W. Hoyer, W. Zheng and J. Luo, *Adv. Sci.*, 2024, **11**, 2308279.
35 G. S. Lee, H. W. Lee, H. S. Lee, T. Do, J.-L. Do, J. Lim, G. I. Peterson, T. Friščić and J. G. Kim, *Chem. Sci.*, 2022, **13**, 11496.
36 G. S. Lee, H. S. Lee, N. Kim, H. G. Shin, Y. H. Hwang, S. J. Lee and J. G. Kim, *Macromolecules*, 2024, **57**, 9408.
37 S. Hou, D. M. Hoyle, C. J. Blackwell, K. Haernvall, V. Perz, G. M. Guebitz and E. Khosravi, *Green Chem.*, 2016, **18**, 5190.
38 B. Wang, Y. Sun, T. P. Davis, P. C. Ke, Y. Wu and F. Ding, *ACS Sustain. Chem. Eng.*, 2018, **6**, 11704.
39 L. Tran and T. Ha-Duong, *Peptides*, 2015, **69**, 86.
40 M. R. Elkins, T. Wang, M. Nick, H. Jo, T. Lemmin, S. B. Prusiner, W. F. DeGrado, J. Stöhr and M. Hong, *J. Am. Chem. Soc.*, 2016, **138**, 9840.
41 Y. Xiao, B. Ma, D. McElheny, S. Parthasarathy, F. Long, M. Hoshi, R. Nussinov and Y. Ishii, *Nat. Struct. Mol. Biol.*, 2015, **22**, 499.
42 F. Hsu, G. Park and Z. Guo, *ACS Omega*, 2018, **3**, 8401.
43 A. T. Petkova, R. D. Leapman, Z. Guo, W.-M. Yau, M. P. Mattson and R. Tycko, *Science*, 2005, **307**, 262.
44 B. I. Giasson, I. V. J. Murray, J. Q. Trojanowski and V. M.-Y. Lee, *J. Biol. Chem.*, 2001, **276**, 2380.
45 M. Schweighauser, Y. Shi, A. Tarutani, F. Kametani, A. G. Murzin, B. Ghetti, T. Matsubara, T. Tomita, T. Ando, K. Hasegawa, S. Murayama, M. Yoshida, M. Hasegawa, S. H. W. Scheres and M. Goedert, *Nature*, 2020, **585**, 464.
46 I. M. van der Wateren, T. P. J. Knowles, A. K. Buell, C. M. Dobson and C. Galvagnion, *Chem. Sci.*, 2018, **9**, 5506.

47 Y. Yoshimura, Y. Lin, H. Yagi, Y.-H. Lee, H. Kitayama, K. Sakurai, M. So, H. Ogi, H. Naiki and Y. Goto, *Proc. Natl. Acad. Sci. U. S. A.*, 2012, **109**, 14446.
48 M. Kim, Y. Lin, E. Nam, D. M. Kang, S. Lim, Y. K. Kim, Y.-H. Lee and M. H. Lim, *Nat. Chem. Biol.*, 2025, **21**, 1709.
49 S. Park, C. Na, J. Han and M. H. Lim, *Metallomics*, 2023, **15**, mfac102.
50 Y. Yi, B. Kim, M. Kim, Y. H. Ko, J. H. Kim and M. H. Lim, *Chem. Sci.*, 2025, **16**, 4366.
51 I. Benilova, E. Karran and B. De Strooper, *Nat. Neurosci.*, 2012, **15**, 349.
52 J. Han, J. Yoon, J. Shin, E. Nam, T. Qian, Y. Li, K. Park, S.-H. Lee and M. H. Lim, *Nat. Chem.*, 2022, **14**, 1021.
53 K. W. Dunn, M. M. Kamocka and J. H. McDonald, *Am. J. Physiol. Cell Physiol.*, 2011, **300**, C723.